

## POSITRON EMITTERS PRODUCED FROM NATURALLY OCCURRING TARGETS

T. W. Leadbeater<sup>†</sup>, A. Buffler, T. Hutton, M. van Heerden, Metrological and Applied Sciences  
 University Research Unit, Department of Physics, University of Cape Town, South Africa

### Abstract

Short lived positron emitters are used as flow following tracer particles in the study of dynamic processes within physics and engineering applications. For full representation of the materials of interest, tracer particles must be activated with proton rich radionuclides utilising reactions on their naturally abundant isotopic content. Cyclotron accelerated alpha particle beams incident upon (<sup>16</sup>O) oxygen rich targets have been investigated in producing the positron emitter <sup>18</sup>F within naturally occurring materials.

Simulations and numeric calculations of the beam conditions are used to maximise the activation yield and minimise heat load by carefully placing the Bragg peak in relation to the water-cooled target. Corresponding to the target thickness, the 100 MeV extraction energy is degraded to match a broad resonance in <sup>18</sup>F production around 35 MeV, while maintaining energy above the 18 MeV threshold. Beam currents below 1 microamp resulted in typical <sup>18</sup>F yields of 1 - 2 mCi within spherical SiO<sub>2</sub> targets of diameters 1 - 10 mm, ideal for envisaged application studies.

### INTRODUCTION

Positron emitting species are used in the non-invasive investigation and radiological imaging of dynamic physical and engineering systems, and those of industrial interest. Materials representation is critical in these applications, requiring the positron emitting species to be produced within naturally occurring materials as it is infeasible to use isotopically enriched targets for this purpose. Production of the medically significant positron emitting radioisotopes uses a range of different target systems and natural or isotopically enriched targets. The focus of this article is on <sup>18</sup>F production with naturally occurring solid targets. Production of <sup>18</sup>F and other isotopes within the context of this work are summarised in Table 1.

The predominant production of <sup>18</sup>F (110 minute half-life) results in free <sup>18</sup>F<sup>-</sup> ions in aqueous solution (the use of gaseous targets is excluded in this discussion), with the majority of conventional global production prepared by irradiating <sup>18</sup>O-water targets. The resultant solution can be processed chemically, leading to the vector molecules of diagnostic imaging (including for example 18-fluorodeoxyglucose (<sup>18</sup>FDG)), or other materials used as radiological tracers. Similarly, <sup>68</sup>Ge offers a convenient radiochemical synthesis route, being produced from a solid target loaded onto a SnO<sub>2</sub> based separation column. The long lived (271 day half-life) <sup>68</sup>Ge decays via electron capture to the short lived <sup>68</sup>Ga (68 minute half-life) which collects as free <sup>68</sup>Ga<sup>3+</sup> ions in liquid form within the column. In the cases of both <sup>18</sup>F and <sup>68</sup>Ge<sup>3+</sup>, the ions can be extracted, concentrated, and

processed radiochemically to produce tracer substances and radiopharmaceuticals as required by the imaging application in question. These techniques have been utilised in imaging physical and industrial systems with success, however they suffer from questionable species representation and often cannot survive the harsh conditions (e.g., temperatures, pressures, and chemical environment) they are subjected to in such devices.

Table 1: Reactions and Targets (adapted from Ref. [1])

Reaction	Target	State, % abundance	Energy range [MeV]
<sup>18</sup> O(p, n) <sup>18</sup> F	H <sub>2</sub> <sup>18</sup> O, <sup>18</sup> O <sub>2</sub>	Liquid, 0.2	18 - 4
<sup>16</sup> O( <sup>3</sup> He, p) <sup>18</sup> F	<sup>nat</sup> H <sub>2</sub> O	Liquid, 99.7	15 - 1
<sup>16</sup> O( <sup>3</sup> He, n) <sup>18</sup> Ne → <sup>18</sup> F			40 - 15
<sup>16</sup> O(α, np) <sup>18</sup> F	<sup>nat</sup> H <sub>2</sub> O,	Liquid /	40 - 20
<sup>16</sup> O(α, 2n) <sup>18</sup> Ne → <sup>18</sup> F	<sup>nat</sup> SiO <sub>2</sub>	Solid, 99.7	
<sup>16</sup> O(α, d) <sup>18</sup> F			
<sup>40</sup> Ca(α, p) <sup>43</sup> Sc	<sup>nat</sup> Ca	Solid, 96.9	~ 50
<sup>40</sup> Ca(α, n) <sup>43</sup> Ti → <sup>43</sup> Sc			
<sup>nat</sup> Ga(p, xn) <sup>68</sup> Ge	<sup>nat</sup> Ge	Solid, 60.1	< 66

Ideally, for applications in industrial systems, tracer materials produced from the bulk materials of interest are required, such that the imaging or other measurement is truly non-invasive. To this end, the production of <sup>18</sup>F in naturally occurring solid targets has been utilised. At the University of Birmingham, UK, the <sup>3</sup>He reactions are utilised, with <sup>3</sup>He beam of 35 MeV energy and ~ 5 μA beam current. Under these conditions the Birmingham MC40 cyclotron can produce up to 1.5 GBq / 40 mCi of <sup>18</sup>F activity in 3 ml of (<sup>nat</sup>H<sub>2</sub>O) water for radiochemical tracer production, and similar activity on solid targets containing sufficient oxides [1]. The <sup>18</sup>O(p, n)<sup>18</sup>F reaction is used when preparing <sup>18</sup>F in solution to be processed chemically.

The University of Cape Town has established a positron imaging facility used for the study of physical, engineering, and industrial applications on the National Research Foundation (NRF) accelerator facility iThemba LABS (iThemba Laboratory for Accelerator Based Sciences) [2]. The primary tracer isotope used has been <sup>68</sup>Ga, produced from commercial <sup>68</sup>Ge/<sup>68</sup>Ga radioisotope generators manufactured by iThemba LABS. The <sup>68</sup>Ge is extracted and radiochemically treated to produce a wide range of representative tracer materials, often starting from an ion-exchange resin polymer core and modifying the density and surface properties to match those characteristics required by the application and research questions [3]. Recently, <sup>18</sup>F has been extracted from commercial medical supplies of

<sup>†</sup> Tom.Leadbeater@uct.ac.za

Content from this work may be used under the terms of the CC-BY-4.0 licence (© 2022). Any distribution of this work must maintain attribution to the author(s), title of the work, publisher, and DOI

<sup>18</sup>F<sup>18</sup>FDG and used successfully in radiochemically labelling the surface of solid materials for similar applications [4].

For the direct activation of solid materials of industrial interest, we turn to the alpha particle induced reactions on oxide bearing targets utilising the available beams accelerated at iThemba LABS. Fig. 1 shows the cross-sections for the different reaction channels between alpha particles and oxygen-16 up to 100 MeV beam energy. The <sup>18</sup>F producing reactions are highlighted in red, having a threshold at 18 MeV and a broad resonance peaking at around 0.1 barn at 35 MeV. The competing reactions consist mostly elastic and inelastic scattering, and capture reactions leading to short lived (< 2.5 minute half-lives) or stable end products.

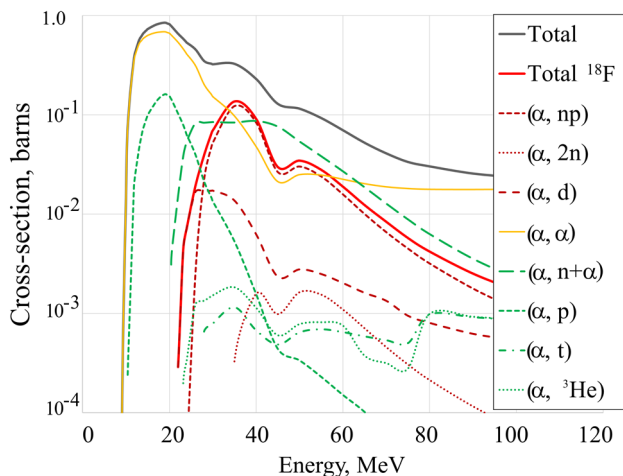


Figure 1: Interaction cross-sections for <sup>16</sup>O( $\alpha$ , x) [5].

### BEAMLINE CONSIDERATIONS

For irradiation, helium ions are produced in the ECR ion source and accelerated to 8 MeV using the solid pole injector cyclotron. The beam is then injected into the  $k = 200$  Separated Sector Cyclotron (SSC) of iThemba LABS and accelerated to 100 MeV. Following extraction of the beam from the SSC, it is directed through a set of beam delivery lines using a  $k = 100$  switching magnet and delivered to horizontal target station 1. The target system consists of a target holder designed to hold the target capsule in the irradiation position and to provide cooling in the form of water circulation. The target capsule contains the material to be irradiated, in this case in the form of SiO<sub>2</sub> based glass beads of diameters ranging from 1 – 10 mm. The target capsule, mounted in the holder, and target holder are manipulated robotically to place them inside target station 1, which provides the interface between the beam delivery line vacuum and water-cooled environment of the target volume. In passing from the beamline vacuum to the target material the beam traverses structural materials in the form of entrance/exit windows and the cooling layers. The beam exits the vacuum through two 25  $\mu$ m Havar foils (ICRU-470 / UNS R30004) separated by a 10 mm helium gas flow maintained at 1.2 bar pressure. A 4.0 mm air gap separates the final Havar exit window and a 0.5 mm thick aluminium layer serving as the entrance window to target station 1.

Inside the target station a circulating water flow at 10 bar pressure and 30 l/min flow rate cools the target holder, capsule and aluminium beam stop positioned behind the target capsule. In this work a perforated target capsule was used, allowing the flow of cooling water into the capsule, and immersing the target spheres. The direct contact of coolant with the target serves two purposes: to increase efficiency of heat removal from the material, and to agitate and/or rotate the targets increasing the effective irradiation area. A schematic of the layers the beam passes through in reaching the beam stop is shown in Fig. 2.

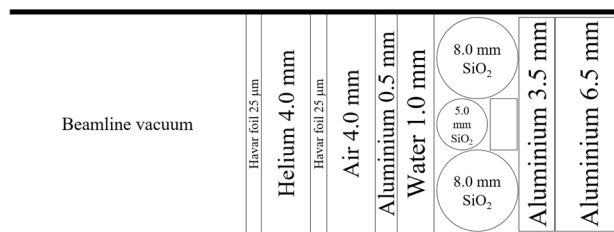


Figure 2: Target stack and material layers.

Numerical modelling for the target stack described above has been used to calculate the residual energy and energy deposition curves shown in Fig. 3. The perforated target capsule has not been included, assuming that the beam passes unhindered through this layer apart from the occupying water. The model proceeds by calculating successive energy loss per 10  $\mu$ m linear path length through the given material for the current energy of the beam at that position. The beam energy is calculated using a linear interpolation between entries in the stopping power tables taken from the NIST stopping power and range tables for helium ions [6].

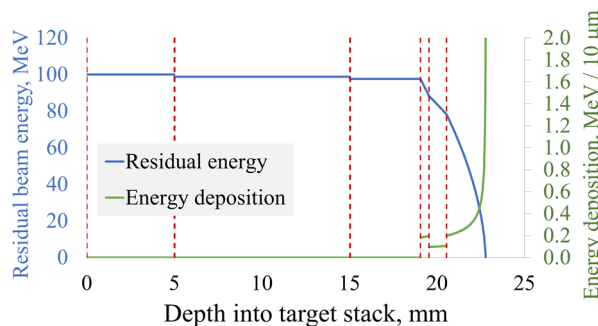


Figure 3: Energy and energy loss per 10  $\mu$ m linear depth.

The numerical modelling is consistent with a Monte Carlo approach constructed using SRIM/TRIM. Fig. 3 shows the residual energy (MeV) (blue curve) defined as the beam energy remaining after traversing the given thickness of material in the target stack, where zero is defined as the edge of the beamline vacuum and the initial energy is 100 MeV. The energy deposition per unit 10  $\mu$ m linear path length is shown on the same horizontal scale (green curve), illustrating the layers where energy deposition is enhanced due to materials differences (density and proton number) between layers, the Bragg peak near the end of the particle range is clearly visible. The boundaries between target stack layers are shown in red.

## TARGET CONSIDERATIONS

It is useful to consider the energy and energy loss in more detail within the SiO<sub>2</sub> target material, for the beam having already traversed the dead layers of the target stack. These data are presented in Fig. 4, where the depth is now measured relative to the front surface of the target and the residual beam energy entering the target is approximately 80 MeV from a 100 MeV extraction. Under these conditions the maximum linear penetration depth of the beam into the target is around 2.3 mm. In Fig. 4 the energy loss curve is shown as a proxy to heat deposition by the beam, with the majority of heating occurring within the Bragg peak at the end of the trajectory. The expected <sup>18</sup>F yield is shown as the red curve, calculated by convolving the microscopic cross sections for production in Fig. 1 with the beam energy at the given depth within the target. The yield is given in arbitrary units, where calibration to absolute units depends on target density and beam conditions and is left as further work. The grey shaded region illustrates the region where the majority of activation is produced (the resonance peak shown by the dotted line), with the beam energy dropping below the threshold limit for production (dotted line) after penetrating 2 mm into the target. The yellow shaded region therefore shows the region within the target where the beam serves solely to heat the target without producing useful activation species (and area under the green and red curves serves as proxy to target activation and heating respectively).

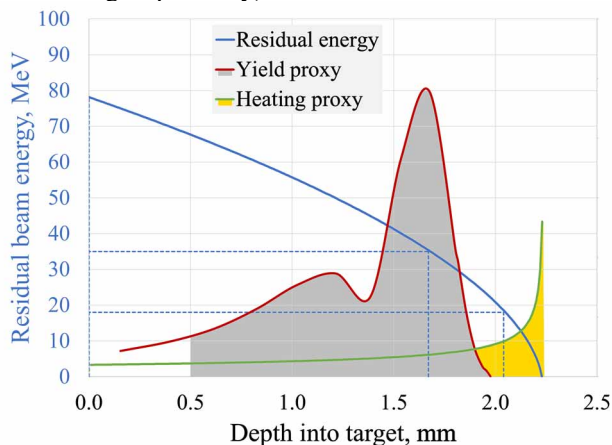


Figure 4: Energy, energy loss, and expected <sup>18</sup>F yield per 10 μm linear depth into the target material only.

An optimisation approach can be considered, where the activation curve (grey) is placed within the target material and the heating curve (yellow) is placed outside of the target and in the cooling water or aluminium beamstop. The optimisation is achieved by altering the beam energy to match the dimensions of the target for the specific activation. In practice the beam energy delivered by the SSC remains at the 100 MeV maximum that can be delivered to the target station (limited by the  $k = 100$  switching magnet), and is degraded by placing aluminium absorbers of different thicknesses within the target stack upstream of the target capsule. Fig. 5 illustrates the calculated optimisation for the range of alpha particle energies possible from the

SSC (200 MeV – 75 MeV) where the lower energy is that which barely penetrates into the target layer when using the current target stack. The 100 MeV beam (red curve) produces useful activation yield up to 2 mm depth, limiting the maximum diameter of the target to this value when keeping the heating outside of the target. The optimal beam energy when leaving the target is around 20 MeV to maximise yield and minimise heating. To optimally activate larger targets higher incident beam energy or a redesigned target stack would be required.

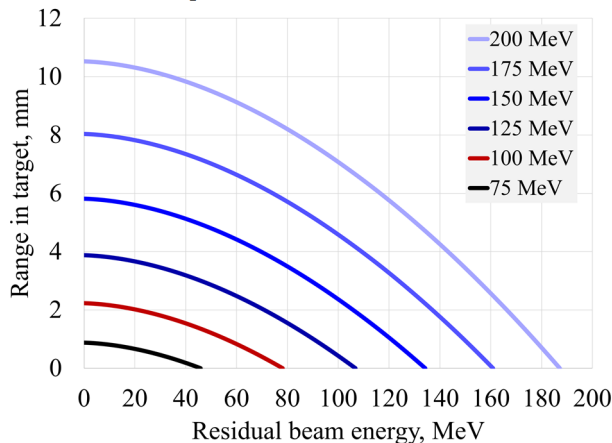


Figure 5: Range into target for incident beam energy.

The linear position along the target stack where the maximum <sup>18</sup>F yield is expected to be produced (blue points), and the maximum thickness of target where the heat deposition curve is placed outside of the target material (green) for the range of initial beam energy considered is shown in Fig. 6.

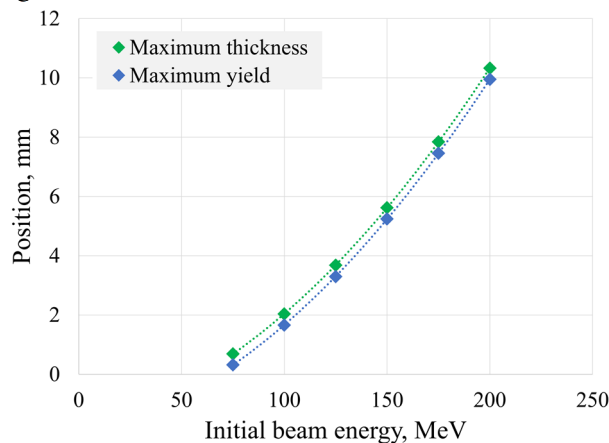


Figure 6: Range into target for incident beam energy.

The zero position is taken as the front face of the SiO<sub>2</sub> target material, and quadratic fits are shown to guide the eye. It is clear from these data that the maximum thickness of target increases with increasing beam energy, and that the region of maximum activation occurs close to the back surface of the target, it is therefore advantageous to enable rotation of the target within the beam to distribute the production yield while maintaining the heat load outside of the material.

In practice it is possible to activate larger targets to a surface layer, with the beam fully stopping within the target provided that it can survive the beam heating. The circulating cooling water has the advantage of agitating the target spheres and seems to provide rotation, enabling isotropic beam entry relative to the target centre, thus distributing activation yield and heat load through the target. For the larger spheres the heat load limits the beam current that can be delivered without damaging the materials. A simple reaction rate activation model has been used to estimate the expected  $^{18}\text{F}$  yield, using the parameters as delivered experimentally [7]. An average microscopic production cross-section for total  $^{18}\text{F}$  production of 12 mb and beam current of 0.8  $\mu\text{A}$  incident for 2 hours is considered. The target density is 2.5  $\text{g cm}^{-3}$ , and thickness 0.1 cm. For our beam and target conditions the expected yield is then around 2 mCi. A more advanced model building on the energy loss calculations outlined above is left for future work. Experimental campaigns using the target stack as described above, with initial beam energy of 100 MeV and target spheres of diameters ranging from 1 – 10 mm resulted in a total of 24 samples with activities in the 1 – 2 mCi range. Isotopic characterisation measurements confirmed the yield at end of beam to be predominantly  $^{18}\text{F}$  (> 95%) produced by the reactions as described. The experimental results are broadly consistent with the expectations from the modelling. Contaminant positron and gamma emitting species were observed at the percent level, with their origins traced to alpha particle and fast neutron (spallation) interactions with trace amounts of other naturally occurring materials present in the target [7]. The positron emitter  $^{43}\text{Sc}$  was observed at around 5% yield, produced from  $^{40}\text{Ca}$  offering a potential isotope for future work.

Potential applications are targeted towards production of tracer particles used for the study of physical flows and engineering systems using positron emission particle tracking (PEPT). It is desirable for the tracer particle materials to accurately reflect the motion and behaviour of the inactive bulk particles forming the system under study. For most applications, and specifically those of industrial interest, solids of naturally occurring isotopic content are required. For full representation of the materials of interest, tracer particles must therefore be activated with proton rich radionuclides utilising reactions on their naturally abundant isotopic content. Typical PEPT studies are used to measure dynamic and kinematic properties of the tracer particle, which is mixed within the bulk material of the system under study. A single tracer particle may therefore represent the behaviour of many millions and/or many tons of bulk material, with local bulk densities, residence times, and velocity flow fields being of particular interest [8, 9].

## CONCLUSION

A target holding system has been modified to enable  $\text{SiO}_2$  glass spheres of diameters 1 – 10 mm to be irradiated with up to 100 MeV alpha particles using the horizontal target station 1 and separated sector cyclotron of iThemba LABS. The  $^{16}\text{O}(\alpha, x)^{18}\text{F}$  reactions have been explored to

produce the positron emitter  $^{18}\text{F}$  within these naturally isotopically occurring solid materials. Simulations and numerical calculations of the beam conditions have been used to maximise the activation yield and minimise heat load by carefully placing the Bragg peak in relation to the water-cooled target. In correspondence to the target thickness, the 100 MeV extraction energy is degraded to match a broad resonance in  $^{18}\text{F}$  production around 35 MeV, while maintaining energy above the 18 MeV threshold. Beam currents below 1 microamp resulted in activities between 1 - 2 mCi, with around 95% of the yield attributed to  $^{18}\text{F}$ . The activated samples have applications in the technique of positron emission particle tracking, where short lived positron emitters are used as flow following tracer particles. As the tracer is designed to be representative of the bulk materials in question, the positron emitting species must be produced from the naturally occurring isotopic content of the particles, motivating this application.

## REFERENCES

- [1] D. J. Parker, "Positron emission particle tracking and its application to granular media", *Rev. Sci. Instrum.*, vol. 88, p. 051803, 2017. doi: 10.1063/1.4983046
- [2] A. Buffler *et al.*, "PEPT Cape Town: a new positron emission particle tracking facility at iThemba LABS", IAEA, Nuclear Research Applications and Utilization of Accelerators, Proceedings series (International Atomic Energy Agency. CD-ROM) CN-173, IAEA, Vienna, 2010.
- [3] M. van Heerden, A. Buffler, K. Cole, and T. Leadbeater, "Density-modified tracers for positron emission particle tracking", *J. Phys.: Conf. Ser.*, to be published.
- [4] A. Camroodien, M. van Heerden, S. Nair, and T. Leadbeater, "Radiochemistry for Positron Emission Particle Tracking (PEPT)", in *Proc. South African Institute of Physics (SAIP'21)*, Potchefstroom, South Africa, Jul. 2021, pp. 542 – 547. ISBN: 978-0-620-97693-0
- [5] A. J. Koning, D. Rochman, J. Sublet, *et al.*, "TENDL: complete nuclear data library for innovative nuclear science and technology", *Nucl. Data Sheets*, vol. 155, pp. 1-55, 2019. doi:10.1016/j.nds.2019.01.002
- [6] M. J. Berger, M. Inokuti, *et al.*, "Stopping Powers for Protons and Alpha Particles", International Commission on Radiation Units and Measurements (Bethesda Maryland), ICRU Report 49, January 1, 1993.
- [7] T. Leadbeater, A. Buffler, M. van Heerden, A. Camroodien, and D. Steyn, "Development of tracer particles for positron emission particle tracking (PEPT)", *Nucl. Sci. Eng.*, to be published.
- [8] T. W. Leadbeater, D.J. Parker, and J. Gargiuli, "Positron imaging systems for studying particulate, granular and multiphase flows", *Particuology*, vol. 10, no.2, pp. 146-153, 2012. doi:10.1016/j.partic.2011.09.006
- [9] T. Leadbeater, J.P.K. Seville, and D.J. Parker, "On trajectory and velocity measurements in fluidized beds using positron emission particle tracking (PEPT)", *Can. J. Chem. Eng.*, vol. 101, no. 1, pp. 269-282, 2022. doi:10.1002/cjce.24622